Published in final edited form as:
J Am Chem Soc. 2011 August 24; 133(33): 13055–13063. doi:10.1021/ja2024993.

Synthesis and Characterization of Three-Coordinate Ni(III)-Imide Complexes

Vlad M. Iluc[†], **Alexander J. M. Miller**[†], **John S. Anderson**[†], **Marisa J. Monreal**[‡], **Mark P. Mehn**[§], and **Gregory L. Hillhouse**[†,*]

[†]Gordon Center for Integrative Science, Department of Chemistry, University of Chicago, Chicago, Illinois 60637

[‡]Department of Chemistry & Biochemistry, University of California, Los Angeles, California 90095

[§]Division of Chemistry and Chemical Engineering, Arnold and Mabel Beckman Laboratories of Chemical Synthesis, California Institute of Technology, Pasadena, California 91125.

Abstract

A new family of low-coordinate nickel imides supported by 1,2-bis(di-*tert*-butylphosphino)ethane was synthesized. The oxidation of nickel(II) complexes led to the formation of both aryl- and alkyl-substituted nickel(III) imides, and examples of both types have been isolated and fully characterized. The aryl substituent that proved most useful in stabilizing the Ni(III)-imide moiety was the bulky 2,6-dimesitylphenyl. The two nickel(III)-imide compounds showed different variable-temperature magnetic properties, but analogous EPR spectra at low temperatures. In order to account for this discrepancy, a low-spin/high-spin equilibrium was proposed to take place for the alkyl-substituted imide nickel(III) complex. This proposal was supported by DFT calculations. DFT calculations also indicated that the unpaired electron is mostly localized on the imide nitrogen for the nickel(III) complexes. The results of reactions carried out in the presence of hydrogen donors supported the findings from DFT calculations that the adamantyl substituent was a significantly more reactive hydrogen-atom abstractor. Interestingly, the steric properties of the 2,6-dimesitylphenyl substituent are important not only in protecting the Ni=N core but also in favoring one rotamer of the resulting nickel(III) imide, by locking in the phenyl ring in a perpendicular orientation with respect to the NiPP plane.

Introduction

Although a plethora of nickel complexes has been studied and characterized, isolating low-coordinate species that feature multiple bonds between nickel and a light element is still challenging. A strategy used by our group has been to employ the dtbpe ligand (dtbpe = 1,2-bis(di-*tert*-butylphosphino)ethane), which increases the steric congestion around the metal center. This ancillary ligand, which is also a strong σ donor, is efficient in stabilizing electron-deficient nickel centers.[1-8] DFT calculations suggest that the lowest unoccupied molecular orbital of the [(dtbpe)Ni^{2+}] fragment, a 12 e^- species, is a $p_y/d_{x^2-y^2}$ hybrid of π symmetry. This low-lying, empty orbital can interact with π donors to generate multiple bonds with the metal center. Based on this scaffold, three representative complexes, with the generic formula (dtbpe)Ni=X (X = NR, PR or CR_2), were synthesized.[1-3] Those unusual examples of terminal-imide, -phosphinidene, and -carbene ligands for a late-transition metal

*Corresponding author g-hillhouse@uchicago.edu .

Supporting Information Available. Experimental details for compound characterizations, DFT calculation details, and full crystallographic descriptions (as cif) are available free of charge via the internet at http://pubs.acs.org.

allowed insight into the intermediates proposed in group-transfer reactions and in coupling processes.[4-6] They also showed unique reactivity in small molecule activation including olefin functionalization.[7, 8]

Although Ni(II)=X moieties were synthesized and characterized, Ni(III)-imide complexes had been predicted to be unstable on the basis of the high oxidation state of nickel and the existence of a multiple bond between nickel and nitrogen. Herein we present a comprehensive study on the synthesis and characterization of Ni(III)-imide complexes supported by the dtbpe ligand. The use of a large substituent at the nitrogen, 2,6-(2,4,6-$Me_3C_6H_2)_2C_6H_3$ (dmp), increased the stability of the corresponding nickel(III) imide. One of the nickel(III)-imide complexes displayed interesting magnetic properties that were investigated both in solution and the solid state. Accordingly, the alkyl- and aryl-substituted Ni(III)-imides display distinct reactivity patterns: the alkyl imide is a potent H-atom abstractor, reacting rapidly with ethereal solvents, while the aryl imide is stable in ethers but does accept a hydrogen atom from a tin hydride.

Results and discussion

Synthesis and characterization of Ni(III) imide complexes

Prior to this work, only one example, the neutral Ni(III) imide (Me_3NN)Ni=NAd (Me_3NNH = N,N-(1,3-dimethylpropanediylidene)dimesitylaniline) had been reported.[9] Initial attempts to isolate a cationic Ni(III) imide by the one-electron oxidation of the Ni(II) imide (dtbpe)Ni=NAd (**1**)[10] with the ferrocenium salt $[Cp_2Fe^+][B(Ar^F)_4^-]$ (Ar^F = 3,5-bis(trifluoromethyl)phenyl) in a diethyl ether solution (Scheme 1) led to the formation of $[(dtbpe)NiNHAd^+][B(Ar^F)_4^-]$ (**2**), a Ni(II) amide complex. A reactive Ni(III) imide, **3**, is proposed as an intermediate, which converts to **2** in the presence of an external hydrogen atom donor (Scheme 1). The same product, **2**, was also isolated from the reaction of the Ni(I) triflate (dtbpe)NiOTf (**4**)[11] with adamantyl azide in diethyl ether, followed by $[TfO^-]$/$[B(Ar^F{}_4)^-]$ anion exchange (Scheme 1). A Ni(I) cationic azide complex was envisioned to give **3**, which led again to **2**.

The Ni(II) amide **2** was characterized by single-crystal X-ray diffraction (Figure 1). Two independent molecules were found in the unit cell. The metal center and the nitrogen atom are trigonal planar (the sum of angles around Ni is 359.4° and around N is 356.0°). The Ni–N average distance of 1.765(5) Å is longer than the analogous distance in the nickel(II) imide (dtbpe)Ni=NAd (1.673(2) Å).[10] The NiNC angle of 135.77° (average value) indicates an sp^2 hybridization of the nitrogen atom and a possible π interaction between nickel and nitrogen. The amide hydrogen was found in the electronic density map at 0.903 Å from nitrogen and refined isotropically.

A cyclic-voltammetry study of **1** in THF showed complex redox behavior. In order to avoid side reactions (Scheme 1) and eliminate the presence of possible hydrogen-atom sources, the solvent was replaced with 1,2-difluorobenzene (DFB), which, although polar, is less reactive than THF. In DFB, the cyclic voltammogram of **1** (Figure 2) features two reversible waves, which were assigned to the Ni(III)/Ni(II) and Ni(II)/Ni(I) couples (−1.07 V and −1.43 V, respectively, both values are relative to Cp_2Fe/Cp_2Fe^+). These observations indicated that the isolation of a Ni(III) imide species might be achieved in the absence of reactive solvents.

The oxidation of **1** was repeated in extensively purified DFB. Extreme caution was used to avoid the presence of any contaminant (including diethyl ether and THF). Consequently, the absence of any possible hydrogen-atom sources allowed the isolation of a paramagnetic, purple, crystalline powder, $[(dtbpe)Ni{=}NAd^+][B(Ar^F)_4^-]$ (**3**), in good yield (Scheme 1). Complex **3** was unstable in the presence of diethyl ether or THF, in which it converted

rapidly and quantitatively to the Ni(II) amide **2** (Scheme 1). It is important to note that **3** represents the first ionic terminal nickel(III) imide and it shows high reactivity versus ether solvents, unlike (Me_3NN)Ni=NAd.[9]

Complex **3** was characterized by single-crystal X-ray diffraction (Figure 3). The metal center is trigonal planar and the nitrogen atom, N, lies in the P(2)–Ni(1)–P(1) plane (the sum of angles around Ni is 359.4°). The Ni–N distance of 1.657(5) Å is only 0.016 Å shorter than in the parent nickel(II) imide, (dtbpe)Ni=NAd (**1**, 1.673(2) Å), and is similar to the corresponding distance in (Me_3NN)Ni=NAd (Ni–N = 1.662(2) Å).[9] Other metrical parameters were also similar for **3** and **1**: the N_{imide}–C bond (1.424(7) Å for **3** and 1.417(3) Å for **1**) and the Ni–N–C angle (164.2(5)° for **3** and 163.0(2)° for **1**). The deviation of this angle from linearity was also observed for an iron alkyl-substituted imide, 159.6(3)° in ($^{i\text{Pr}}$PDI)FeNAd ($^{i\text{Pr}}$PDI = (2,6-^{i}PrC_6H_3N=CMe)$_2C_5H_3N$),[12] although it was 178.51(6)° in ($PhB^{Ph}P_3$)FeNAd ([$PhB^{Ph}P_3$] = [$PhB(CH_2PPh_2)_3^-$. [13, 14]] In general, aryl-substituted imides tend to have a straight Ni–N–C arrangement as a consequence of the extended conjugation provided by the phenyl ring as was reported for (dtbpe)Ni=NMes (Ni–N–C = 180.0°).[10]

Faced with the instability of **3** in ethereal solvents, it was reasoned that a larger substituent on the nitrogen might protect the Ni–N core better than the adamantyl group and decrease its reactivity. We previously employed a similar strategy to stabilize a nickel(II) phosphinidene, (dtbpe)Ni=P(dmp),[2] after several failures to isolate a phosphinidene with a smaller substituent.

Reaction of the Ni(0)-benzene adduct {(dtbpe)Ni}$_2$(μ-C_6H_6) (**5**) with (dmp)N_3[15] led to the isolation, in high yield, of the Ni(0) side-bound azide complex (dtbpe)Ni{η^2-N_3(dmp)}, **6**(Scheme 2). Complex **6** was characterized by ^{1}H, ^{31}P, and ^{13}C NMR, infrared spectroscopy and elemental analysis. The NMR spectra show characteristics of a planar, unsymmetrical Ni(0) complex, with magnetically non-equivalent phosphorous nuclei (J_{PP} = 52 Hz). Its solution structure was assigned by analogy to those of the previously characterized η^2-bound azides (dtbpe)Ni(η^2-N_3Ad) and (dtbpe)Ni(η^2-N_3Mes).[10]

The bulky dmp substituent increased the thermal stability of **6**; both adamantyl and mesityl analogues decomposed when heated for 24 hours at 80 °C. Their thermal conversion to the corresponding imides, **1** and (dtbpe)Ni=NMes, required additive (5%) amounts of **5** to avoid the dissociation of the side-bound azide to **5** and RN_3.[10] Complex **6** is thermally stable and can be heated at 80 °C (C_6D_6) for long periods of time (24 hours) without conversion to the corresponding imide.

Interestingly, crystals of **6** are sensitive to ambient light, which prevented us from determining its solid-state structure but hinted at photochemical reactivity. Exposure of **6** to 254 nm light furnished the corresponding imide, (dtbpe)Ni=N(dmp) (**7**), in quantitative yield after 12 hours at room temperature. Complex **7** has been previously prepared by H• abstraction from (dtbpe)Ni–NH(dmp).[16] No decomposition or side products were observed for this process and **7** was obtained analytically pure. ^{1}H, ^{31}P, and ^{13}C spectroscopic studies of **7** indicated a C_{2v}-symmetric complex in solution, with magnetically equivalent phosphorous nuclei (δ 119.23) matching the previously reported data.[16] The complex **7** is one of the few examples of selective photolytic synthesis of an imide from a discrete azide complex.[17,18] Such conversions of azides to imides are not common for organometallic complexes, likely because side-bound azides are rare.[10, 19-25] Organoazides, RN_3, also undergo photochemical conversion to free nitrenes.[26]

In order to determine the feasibility of oxidizing **7** to the desired Ni(III) imide, its electrochemical behavior was studied. A cyclic voltammogram in THF (Figure 4, the use of DFB was not necessary) featured two reversible waves, one at $E_{1/2}$ = −0.76 V (vs. Fc/Fc$^+$),

corresponding to the Ni^{III}/Ni^{II} couple, and one at $E_{1/2} = -2.81$ V for the Ni^{II}/Ni^{I} redox couple.

Accordingly (Scheme 3), the one-electron oxidation of **7**, carried out in diethyl ether at −35 °C with $[Cp_2Fe^+][B(Ar^F)_4^-]$ as the oxidant, led to the isolation, in high yield, of a purple, paramagnetic powder of the Ni(III) complex $[(dtbpe)Ni{=}N(dmp)^+][B(Ar^F)_4^-]$ (**8**). The same product could be obtained independently from **4** by the reaction with $(dmp)N_3$, followed by $[TfO^-]/[B(Ar^F)_4^-]$ anion exchange (Scheme 3). Complex **8** is stable in common solvents like diethyl ether, tetrahydrofuran, or dichloromethane. As expected because of its paramagnetic nature, **8** was ^{31}P and ^{13}C NMR silent and its ^1H NMR spectrum was very broad and difficult to assign.

The single-crystal X-ray structure (Figure 5) of **8** revealed that the cation has pseudo-C_{2v} symmetry, with equal Ni–P distances (2.2314(11) and 2.2318(11) Å) and similar P–Ni–N angles (133.81(10)° and 135.82(10)°). The Ni–N distance is 1.674(3) Å, about 1% longer than the analogous distance found in $[(dtbpe)Ni{=}NAd^+]$ (**3**) or $(Me_3NN)Ni{=}NAd$.[9] A major difference between the two adamantyl-substituted Ni(III) imides (**3** and $(Me_3NN)Ni{=}NAd$) and **8** is the Ni–N–C angle; this angle is almost linear (178.4(3)°) in **8**, perhaps indicative of π delocalization in **8** not possible in **3** or $(Me_3NN)Ni{=}NAd$. A similar pattern was observed for the Ni(II) imides, with the aryl-substituted imides having a larger Ni–N–C angle than the alkyl-substituted complexes.[1,10,16] The greater degree of electron delocalization is also manifested in the slightly shorter N–C bond found in **8** (1.359(5) Å) than in **3** (1.424(7) Å) and $(Me_3NN)Ni{=}NAd$ (1.422(3) Å).[9]

Magnetic susceptibility and EPR spectroscopy studies of Ni(III) imide complexes

The ^1HNMR spectrum (CD_2Cl_2, 25 °C) of the adamantyl complex **3** showed broad resonances, indicative of a paramagnetic species. The solution magnetic moment ($\mu_{eff} = 2.79\ \mu_B$), measured by the Evans method[27, 28] at room temperature, was too high for a low-spin, d^7-Ni(III) complex.[29] Moreover, the solution magnetic moment increased to 3.50 μ_B when the temperature was raised to 345 K. It is noteworthy that the value measured at 345 K is lower than that expected for a quartet state (spin only: $\mu_S = 3.87\ \mu_B$; $\mu_{S+L} = 5.20\ \mu_B$; commonly observed: $\mu_{obs} = 4.30 - 5.20\ \mu_B$).[29]

The temperature dependence of the magnetic moment observed by ^1H NMR spectroscopy for **3** was corroborated by a SQUID solid-state study. The magnetic moment increased from 1.6 μ_B (4 K) to 2.8 μ_B (300 K, Figure 6). The magnetic molar susceptibility did not obey the Curie-Weiss law expected for a mononuclear Ni(III) paramagnet (see the supporting information for details). In order to explain the value of the magnetic moment at low temperatures, two scenarios are proposed: (1) the magnetic moment characterizes a dimeric species, in which the unpaired electrons are antiferromagnetically coupled, and (2) a low-spin/high-spin equilibrium exists. Since crystallographic data (Figure 3) indicated that **3** is a monomer in the solid state, the second interpretation is preferred.

A temperature dependence of the magnetic moment corresponding to the two spin states was calculated by roughly fitting the data with expected values of the magnetic moments. A value of 1.9 μ_B was employed for the doublet state and one of 4.8 μ_B for the quartet state. The molar fraction ([LS] and [HS]) of these two species was calculated as a function of temperature, therefore a temperature-dependent equilibrium constant, K, could be found (Eq. 1).

$$K=\frac{[HS]}{[LS]}=\frac{[HS]}{1-[HS]} \quad \text{where} \quad [HS]=\frac{\mu_{\exp}^2-\mu_{LS}^2}{\mu_{HS}^2-\mu_{LS}^2} \tag{1}$$

The enthalpy change, ΔH = 2.5 kJ/mol, and the entropy ΔS = 1.5 J·mol^{-1}·K^{-1}, can be calculated by interpolating the linear part of the lnK vs. 1/T plot with a first order equation (see Supporting Information). The enthalpy corresponds to a small energy gap between the two states (about 210 cm^{-1}), hence the low concentration of the high-spin species; the very small entropy is typical for a system in equilibrium (no sharp spin cross-over temperature). The resulting equilibrium corresponds to a high-spin: low-spin ratio of about 1:4 at room temperature.

This interpretation is supported by the fact that the EPR X-band spectrum of **3** (3.5 mM in CH_2Cl_2) at 3.7 K is consistent with the presence of a nickel(III) center with a low-spin, d^7 electronic configuration (Figure 7).[30] The spectrum exhibits a single feature lacking a hyperfine structure and is nearly axial with g_1 (2.11) > g_2 (2.02). Another axial feature of low intensity was observed in the half-field region (g ~ 4).

Unlike **3**, complex **8** has a magnetic moment of 1.9 μ_B, measured by the Evans method[27, 28] in CD_2Cl_2 at room temperature, indicative of one unpaired electron and a low-spin Ni(III) species. The solid-state SQUID measurements confirmed the solution data. The magnetic moment (μ_{eff} = 1.8 μ_B, 4 K) did not vary greatly with the temperature (Figure 8) and the magnetization followed the Curie-Weiss law for a mononuclear paramagnetic species, with a Curie temperature, T_C, of 2.78 K and a magnetization constant of 0.357 emu.

Similar to what was observed for the Ni(III) cationic adamantyl imide **3**, the EPR spectrum of **8** (1 mM frozen glass in toluene, Figure 9) shows a single feature, characterized by the parameters g_1 = 2.17, g_2 = 2.06, and g_3 = 1.97. No hyperfine coupling with the nitrogen atom was observed and the signal lost intensity with the increase of temperature.

DFT calculations

The difference in the magnetic behavior of the alkyl- (**3**) and the aryl-substituted (**8**) Ni(III) imides may arise from the electron donating properties of the dmp group, which can lower the energy of the bonding π orbitals and, therefore, increase the low-spin/high-spin energy gap. In order to verify this hypothesis, DFT studies were undertaken. In addition, DFT studies might provide insight into whether the difference in the stability of the two complexes is a consequence of steric or electronic factors. We were unable to isolate other Ni(III) aryl-substituted imides: clean products were not obtained on oxidation of (dtbpe)Ni=NAr (Ar = 2,6-di-*iso*-propylphenyl) or (dtbpe)Ni=NMes failed, possibly due to aryl radical coupling.[31]

DFT calculations were performed on a phenyl-substituted Ni(II)-imide model compound, (dmpe)Ni=NPh (dmpe = $Me_2PCH_2CH_2PMe_2$), such that the role of steric factors is minimized. The geometry-optimization results indicated that the electronic barrier to rotation around the N–C_{ipso} bond is 3.5 kcal/mol. Using the same calculation parameters we investigated both an alkyl-substituted Ni(III)-imide model, [(dmpe)Ni=NC$(CH_3)_3^+$], and an aryl-substituted model, [(dmpe)Ni=NPh$^+$]. For the latter, both the high-spin and the low-spin energies of the two rotamers were calculated.

The free-energy difference between the high-spin and the low-spin isomers of the alkyl-substituted Ni(III) cation is 0.8 kcal/mol (the calculated enthalpy for this process is ΔH = 0.6 kcal/mol). For the aryl-substituted Ni(III) cation, the energy difference between the two spin

states is 4.8 kcal/mol for the rotamers with the aryl ring perpendicular to the NiPP plane and 3.4 kcal/mol for the rotamers with the coplanar ring (Figure 10). The trend indicated by these values is consistent with the fact that the high-spin state can be accessed for the adamantyl Ni(III) imide at room temperature, while only the low-spin state is observed for the corresponding dmp complex, as indicated by the higher energy difference between the low- and the high-spin states of [(dmpe)Ni=NPh$^+$] than of [(dmpe)Ni=NC(CH$_3$)$_3$$^+$]. Interestingly, the free-energy difference between the low-spin state of the rotamer with the phenyl ring perpendicular to the PNiP plane and the high-spin state of the other rotamer was calculated to be only 0.2 kcal/mol. The fact that a transformation between the two was not observed experimentally indicates that the dmp substituent does not rotate freely in solution.

DFT calculations were also used to investigate why the nickel(II) imide (dtbpe)Ni=NAd (**1**) and the corresponding nickel(III) imide [(dtbpe)Ni=NAd$^+$][B(Ar^F)$_4$$^-$] (**3**) show, within experimental error, identical metrical parameters. Three bonding interactions (one having σ symmetry, an in-plane π bond, and an out-of-plane π bond) and an antibonding π interaction (HOMO) were observed for the model compound (dmpe)Ni=N^{t}Bu (Figure 11). A one-electron oxidation would decrease the number of electrons in the antibonding orbital (HOMO) and increase the bond order by 0.5. This bond-order increase should be associated with a decrease in the Ni–N distance in the resulting nickel(III) imide. If an oxidation of the nitrogen center (to form [Ni(II)–AdN$^{\bullet-}$]) occurs, however, instead of the metal center ([Ni(III)–AdN^{2-}]), then the unpaired electron would be localized on the nitrogen atom of the imidyl radical, AdN$^{\bullet-}$. Such an electronic structure would not impact dramatically the metrical parameters associated with the nickel center and could explain the similarity observed between the solid-state structures of (dtbpe)Ni=NAd (**1**) and [(dtbpe)Ni=NAd$^+$][B(Ar^F)$_4$$^-$] (**3**).

Consequently, an investigation of the electronic structure for the alkyl and aryl-imide nickel(III) complexes (Figure 12) shows that the spin density is divided between the nickel and the nitrogen centers. For the alkyl imide model, the spin density on the nitrogen atom (69%) is higher than for the aryl complex (53%), consistent with no change in the metrical parameters of the nickel(II) and the corresponding nickel(III) imide compounds. The observed high affinity of the cationic [(dtbpe)Ni=NAd$^+$] (**3**) for hydrogen atoms supports this interpretation. Similar reactivity was observed for the neutral Ni(III) imide complex (Me$_3$NN)Ni=NAd,[9] confirming the high radical character of the nitrogen atom. Rhodium(I)- and iron(III)- and (IV)-imide complexes have been shown to react with hydrogen-donors at the nitrogen center,[32] and in the case of a cationic iron system a detailed thermodynamic analysis suggests the N-H BDE to be ~88 kcal/mol.[32b] Definitive conclusions about the reactivity behavior of these complexes cannot be drawn easily, however, because a Ni(III) center is also expected to show high reactivity and because other reaction pathways involving a radical localized on the metal cannot be excluded. In addition, the fact that the alkyl-substituted imide complex undergoes a high-spin/low-spin equilibrium can affect the reactivity, since high-spin complexes are generally more reactive than low-spin analogues.

With DFT calculations and the reactivity of **3** with ethers both suggesting that there is less spin density localized on the imide nitrogen of the aryl-substituted nickel(III) complex **8** than for the alkyl-substituted model **3**, we set out to probe the hydrogen-atom abstraction ability of **8** with a more reactive H-donor substrate, ^{n}Bu$_3$SnH (Scheme 4).[33] Accordingly, the known cationic Ni(II)-amide complex [(dtbpe)Ni-NH(dmp)$^+$] (**9**) was obtained after stirring the reaction mixture for 12 hours at room temperature in diethyl ether. Complex **9** was also independently synthesized from the Ni(II) imide **7** by protonation with [H(OEt$_2$)$_2$][B(Ar$_F$)$_4$] (Scheme 4). Interestingly, **7** can be accessed from **8** by reduction with KC$_8$ in diethyl ether (Scheme 4).

Conclusions

A new family of amides and imides supported by the bulky dtbpe ligand and containing a nickel center in different oxidation states was synthesized and characterized. The oxidation of nickel(II) imides allowed the synthesis of corresponding nickel(III) imide cations. Two such complexes were described, an alkyl- (**3**) and an aryl-substituted (**8**) imide. The 2,6-dimesitylphenyl substituent (dmp) proved useful in stabilizing the Ni(III)-imide complex **8**. The two complexes (**3** and **8**) showed different variable-temperature magnetic behaviors but analogous EPR spectra at low temperatures. The effective magnetic moment for **3** increased with the increase in temperature, while it remained constant for **8**. In order to account for this difference, a low-spin/high-spin equilibrium was proposed to take place for **3** but not for **8**. That proposal was supported by DFT calculations. DFT calculations were also used to explain the similarity between the metrical parameters observed for the adamantyl-substituted nickel(II) and nickel(III) imides. Calculations on the model complex (dmpe)Ni=N^{t}Bu showed that three bonding interactions (one having σ symmetry, an in-plane π bond, and an out-of-plane π bond) and an antibonding π interaction (HOMO) constitute the frontier orbitals, resulting in a bond order of 2 for the Ni–N moiety. The removal of an electron from HOMO would result in the shortening of the nickel–nitrogen distance if the unpaired electron is localized on the nickel center, but it would not induce a change in metrical parameters if the unpaired electron were localized on the imide nitrogen. Calculations on an alkyl-imide nickel(III) model complex indicated that the spin density was shared by nickel and the imide nitrogen, with a large component on the nitrogen atom. A similar situation was observed for the aryl-imide nickel(III) simplified model complex, but with a diminished component of the spin density on the nitrogen atom. Reactivity studies in the presence of hydrogen donors supported the results of DFT calculations, and implied that the alkyl-substituted imide **3** is a much more potent H-atom abstractor than the aryl derivative **8**. Interestingly, the steric properties of the dmp substituent are important not only in protecting the Ni=N core but also in favoring one rotamer of the nickel(III) imide; this effect is the consequence of locking in the phenyl ring to be perpendicular with respect to the NiPP plane. When the aryl ring is in the NiPP plane (in conjugation with Ni–N π bond), radical delocalization into the aromatic ring results in aryl-aryl coupling.[31] That conformation was correlated with a higher energy difference between the low-spin and the high-spin states than in the case of the alkyl-substituted imide nickel(III) complex.

Experimental Section

Unless noted otherwise, all operations were performed under a purified nitrogen atmosphere in a standard MBraun Lab Master 130 dry box or under an argon atmosphere using high-vacuum and Schlenk techniques. Hexanes, petroleum ether, and toluene were dried by passage through activated alumina and Q-5 columns under nitrogen.[34] CH_2Cl_2 was dried by distillation from CaH_2 or passage twice through activated alumina columns. THF was distilled from a dark-purple THF solution of sodium benzophenone ketyl. Anhydrous diethyl ether was stirred for 24 h over metallic sodium and filtered under nitrogen through an activated alumina plug. Benzene was refluxed under nitrogen over CaH_2 and distilled. CD_2Cl_2 and C_6D_6, were purchased from Cambridge Isotope Laboratory, degassed, dried over CaH_2, transferred under vacuum, and stored over 4 Å molecular sieves. 4 Å molecular sieves, alumina, silica, and Celite were dried under dynamic vacuum overnight at 180 °C. Q-5 was activated by heating at 200 °C under a 5% H_2 in N_2 atmosphere. Unless noted, chemicals were purchased from commercial sources and used without further purification. KC_8,[35] (dmp)N_3,[15] [Cp_2Fe][B(3,5-$(CF_3)_2C_6H_3)_4$],[36] and [(dtbpe)Ni]$_2(C_6H_6)$[37] were prepared according to the literature methods. All NMR spectra were recorded using a Bruker DRX-400 or DRX-500 spectrometer. ^{1}H NMR spectra were referenced to solvent residual peaks at δ 7.15 for C_6D_6, and δ 5.32 for CD_2Cl_2. ^{31}P NMR spectra was measured using a

250 ppm window and offset referenced to an external standard, 85% phosphoric acid (δ 0.00). ^{13}C NMR spectra were acquired using the pulse-Fourier technique. Proton-decoupled spectra were collected with Waltz decoupling. ^{13}C NMR spectra were referenced to solvent residual peaks, δ 128.0 for C_6D_6 and δ 53.8 for CD_2Cl_2. Infrared spectra were measured as Fluorolube-S20 or Nujol mulls between CaF_2 or KBr plates using a Nicolet 20-SXB spectometer with TGS detector. Solution magnetic susceptibilities were calculated following the Evans method[27, 28] using trimethylsilyl ether as an internal standard. Elemental analyses were performed by Columbia Analytics (Tucson, AZ) or by Midwest Microlab (Indianapolis, IN). Cyclic voltammetry experiments were carried out on an Eco-Chemie Autolab potentiostat using a 0.3 M THF or difluorobenzene (DFB) solution of $[^nBu_4N][PF_6]$ as the electrolyte. DFB was refluxed over CaH_2 and distilled under nitrogen. A ceramic patterned electrode with a platinum working electrode and Ag/AgCl reference electrode from Pine Research Instrumentation was used for data collection. Electrochemical response was recorded using an Eco-Chemie Autolab potentiostat (pgstat20) and GPES 4.3 software. The IR correction drop was not utilized, as there was no significant resistance in solution. The spectra were recorded under a N_2 atmosphere, and for **1** the dry box was purged extensively to avoid any exposure to Et_2O or THF residual vapors. EPR spectra were collected on a Bruker EMX EPR spectrometer. Magnetic-susceptibility measurements were carried out on batches obtained independently until at least two different experiments gave superimposable results. Magnetic-susceptibility measurements were recorded using a SQUID magnetometer at 5000 G. X-ray diffraction data were collected on a Siemens platform goniometer with a charged coupled device (CCD) detector. Structures were solved by direct methods using the SHELXTL (version 5.1) program library (G. Sheldrick, Bruker Analytical X-ray Systems, Madison, WI).[38] All atoms were refined anisotropically and hydrogen atoms were placed in calculated positions unless specified otherwise. Tables with atomic coordinates and equivalent isotropic displacement parameters are listed in the cifs in the supporting information. The crystals were coated with oil (STP Oil Treatment) on a glass slide, which was brought outside the glovebox.

Synthesis of [(dtbpe)Ni-NHAd$^+$][B(Ar^F)$_4^-$] (2)

Method A from (dtbpe)Ni=NAd (**1**) by oxidation in Et_2O. In a typical experiment, a scintillation vial was charged in the dry box with a stirring bar, 40 mg (0.076 mmol) of (dtbpe)Ni=NAd (**1**), and 5 mL of diethyl ether, then cooled to − 35 °C. A cold, blue solution of $[Cp_2Fe^+][B(Ar^F)_4^-]$ (80 mg, 0.076 mmol) in diethyl ether was added to the first solution and the reaction mixture was stirred for 1 h, dried under reduced pressure, and washed with petroleum ether. The products were extracted with diethyl ether and crystals were obtained by layering this solution with petroleum ether. Yield: (96 mg, 80%). **Method B** (from [(dtbpe)Ni=NAd$^+$][B(Ar^F)$_4^-$] (**3**)). 50 mg (0.036 mmol) of **3** were dissolved in 5mL Et_2O or THF. The reaction solution was stirred at room temperature for 30 min. Removing the solvent under reduced pressure yielded 50mg of analytically pure **2** (100% yield). **For 2:** ^{1}H NMR (22 °C, 500 MHz, CD_2Cl_2): δ 8.21 (br, 1H, N*H*), 7.73 (s, 8H, $C_6H_3(CF_3)_2$), 7.56 (s, 4H, $C_6H_3(CF_3)_2$), 2.00 (s, 3H, Ad), 1.79-1.58 (m, 12H, Ad), 1.41 (d, 36H, $C(CH_3)_3$), 1.3 (m, 4H, C_2H_4). ^{31}P{^{1}H} NMR (22 °C, 161.97 MHz, CD_2Cl_2): δ 117.0 (s). ^{13}C{^{1}H} NMR (22 °C, 100.61 MHz, CD_2Cl_2): δ 160.31 (q, C_{Ar}), 135.11 (s, C_{Ar}), 130.21 (s, C_{Ar}), 129.41 (m, CF_3), 128.90 (t, C_{Ar}), 48.1 (s, C_{Ad}), 38.3 (t, C_{Ad}), 36.2 (s, C_{Ad}), 36.38 (d, $C(CH_3)_3$), 35.21 (d, $C(CH_3)_3$), 32.4 (s, C_{Ad}), 30.52 (s, $C(CH_3)_3$), 30.06 (s, $C(CH_3)_3$), 22.3 (m, CH_2). IR: 3224 cm^{-1} (m, ν_{NH}). Anal. (%) for $C_{60}H_{68}F_{24}BNNiP_2$: calcd. C, 51.82; H, 4.93; N, 1.01; found C, 51.72; H, 4.81; N, 0.91.

Synthesis of [(dtbpe)Ni=NAd$^+$][B(Ar^F)$_4^-$] (3)

In a scintillation vial in the dry box, crystals of (dtbpe)Ni=NAd (**1**; 38 mg, 0.0795 mmol) were dissolved in 2 mL of 1,2-difluorobenzene and the dark-red solution was cooled to −35

°C. To the cold solution of **1** was added a cold, dark-blue 1,2-difluorobenzene (2 mL) solution of $[Cp_2Fe^+][B(Ar^F)_4^-]$ (70 mg, 0.063 mmol). The reaction mixture darkened to grey and was stirred for 15 min. The mixture was then dried under reduced pressure and washed with petroleum ether (never exposed to diethyl ether) to extract ferrocene. The remaining dark-grey solid (**3**) was extracted with 1.5 mL of 1,2-diflurobenzene. The resulting grey solution was layered with 3 mL of petroleum ether (diethyl ether free) and cooled overnight to yield 82 mg (0.0590 mmol, 75%) of dark crystals of paramagnetic **3** (purple under microscope). ^{1}H NMR (22 °C, 500 MHz, CD_2Cl_2): δ 7.72 (s, 8H, $B(Ar^F)_4$), δ 7.56 (s, 4H, $B(Ar^F)_4$), δ 5.32 (br s, $\Delta\nu_{1/2}$ = 349 Hz, 36H, $-C(CH_3)_3$), 3.42 (br s, $\Delta\nu_{1/2}$ = 236 Hz, 8H, Ad), 0.08 (br s, $\Delta\nu_{1/2}$ = 104 Hz, 5H, Ad), −1.25 (br s, $\Delta\nu_{1/2}$ = 179 Hz, 4H, $-C_2H_4-$). m.p. = 160-165 °C. Anal. (%) for $C_{60}H_{67}F_{24}BNNiP_2$: calcd. C, 51.86; H, 4.86; N, 1.01; found C, 51.78; H, 4.84; N, 0.93.

Synthesis of (dtbpe)Ni{η^2-N$_3$(dmp)} (6)

To a suspension of $\{(dtbpe)Ni\}_2(C_6H_6)$ (**5**, 166.4 mg, 0.2 mmol) in 5 mL of *n*-pentane, a solution of $(dmp)N_3$ (142.2 mg, 0.4 mmol) in 5 mL of *n*-pentane was added at once under stirring at room temperature. The orange-red suspension turned yellow and formed a yellow precipitate. After stirring for 30 min at room temperature, the mixture was filtered and the precipitate washed twice with 2 mL of *n*-pentane. The solids were dried under reduced pressure and a second crop was isolated by cooling the combined mother liquors to −35 °C. Combined yield: 265 mg, 90%. **For 6:** ^{1}H NMR (20 °C, 400.13 MHz, C_6D_6): δ 7.23 (m, 3H, $C_6H_3Mes_2$), 6.89 (s, 4H, $C_6H_2(CH_3)_3$), 1.07 (m, 4H, C_2H_4), 1.01 (d, 18H, J_{HP} = 12 Hz, $C(CH_3)_3$), 0.97 (d, 18H, J_{HP} = 12 Hz, $C(CH_3)_3$). ^{31}P{^{1}H} NMR (20 °C, 202.47 MHz, C_6D_6): δ 96.64 (d, J_{PP} = 52 Hz), 95.22 (d, J_{PP} = 52 Hz). ^{13}C{^{1}H} NMR (20 °C, 125.77 MHz, C_6D_6): δ 136.96 (s), 135.91 (s), 133.43(s), 129.26 (s), 128.93 (s), 127.92 (s), 125.63 (s), 123.76 (s), 33.96 (d, J_{CP} = 10 Hz, CH_2), 33.72 (d, J_{CP} = 10 Hz, CH_2), 30.06 (s, $C(CH_3)_3$), 30.00 (s, $-C(CH_3)_3$), 22.10 (d, J_{CP} = 10 Hz, $C(CH_3)_3$), 21.81 (d, J_{CP} = 10 Hz, $C(CH_3)_3$), 21.33 (s, *o*-$C_6H_2(CH_3)_3$), 21.28 (s, *p*-$C_6H_2(CH_3)_3$). IR (CaF_2, Fluorolube): 2215 (m), 2107 (s), 2095 (s), 1451 (m), 1313 (m), 1604(m), 1203(s), 1182(m), 1154(s), 1102(m), 889 (w), 851 (w), 801 (w) cm^{-1}. Yellow, single crystals were isolated by cooling a concentrated solution of **6** in *n*-pentane at −35 °C. While crystals were inspected under the microscope a vigorous gas evolution was observed. Several attempts were made to collect crystallographic data on these crystals. Although unit cell parameters were determined, an extensive decomposition was observed during the data collection at 100 K. Anal. (%) for $C_{42}H_{65}N_3NiP_2$: calcd. C, 68.85, H, 8.94, N, 5.74; found C, 70.02, H, 8.69, N, 5.45.

Synthesis of (dtbpe)Ni=N(dmp) (7)

Method A (from (dtbpe)Ni{η^2-N$_3$(dmp)}, **6**, by N_2 extrusion). A solution of **6** (220 mg, 0.3 mmol) in 20 mL of hexanes was placed in a glass Schlenk tube. The tube was cooled at −196 °C in liquid nitrogen and evacuated for 30 min. The Schlenk tube was exposed to a high energy ultraviolet lamp (254 nm, 400 W) with air cooling for 12 h with stirring. The yellow solution turned olive green. The volatiles were removed under reduced pressure to yield analytically pure **7** (210 mg, 100%). **Method B** (from $[(dtbpe)Ni=N(dmp)^+][B(Ar^F)_4^-]$, **8**, by reduction). To a cold solution of **8** (158 mg, 0.1 mmol) in 5 mL of Et_2O at −35 °C, was added dropwise a cold suspension of KC_8 (13.5 mg, 0.1 mmol, 2 mL of Et_2O, −35 °C) over an interval of 5 min. The black suspension was warmed up to room temperature and stirred for an additional 30 min. After removing the volatiles under reduced pressure, the residue was extracted with hexanes, filtered through a plug of Celite, and concentrated. The cooling of this concentrated solution to −35 °C yielded analytically pure **7** as green crystals (65 mg, 90%). The purity of the product was verified by NMR spectroscopy and the data compared to the previously reported data.[16]

Synthesis of [(dtbpe)Ni=N(dmp)$^+$][B(Ar^F)$_4$] (8)

Method A (from (dtbpe)Ni=N(dmp) (**7**) by oxidation). To a cold solution of **7** (141 mg, 0.2 mmol) in 5 mL of Et_2O at −35 °C, was added dropwise a cold suspension of [Cp_2Fe^+][$B(Ar^F)_4^-$] (210 mg, 0.2 mmol, 5 mL of Et_2O, −35 °C) over an interval of 5 min. After the addition was finished, the mixture was warmed up to room temperature and stirred for another 30 min. The volatiles were removed under reduced pressure and the residue was triturated 3 times with 10 mL of pentanes. The isolated solids were dried and analytically pure **8** was isolated by cooling a concentrated diethyl ether solution layered with an equal volume of *n*-pentane to −35 °C. Yield: 280 mg (90%). **Method B** (from (dtbpe)NiOTf (**4**) and (dmp)N_3). A 20-mL scintillation vial was charged with 52 mg (0.1 mmol) of (dtbpe)NiOTf (**7**) and 5 mL Et_2O and cooled to −35 °C. To the cold suspension, was added, with constant stirring, dropwise a cold solution of (dmp)N_3 (35.5 mg, 0.1 mmol in 3 mL of Et_2O at −35 °C) over an interval of 5 min. The mixture was stirred for an additional 10 min and a solution of Na[$B(Ar^F)_4^-$] (89 mg, 0.1 mmol) in 3 mL of Et_2O was added at once. The mixture was warmed up to room temperature and stirred for 30 min. After removal of the volatiles under reduced pressure, the residue was extracted with diethyl ether and filtered. Pure, crystalline **8** was isolated by cooling to −35 °C a concentrated solution of **8** in Et_2O layered with equal volumes of *n*-pentane. Yield: 115 mg, 75%. **For 8:** ^{1}H NMR (20 °C, 400.13 MHz, CD_2Cl_2): δ 10.49 (br s, $\Delta_{1/2}$ = 90 Hz, 7H, $-C_6H_3(C_6H_2(CH_3)_3)_2$), 5.87 (br s, $\Delta_{1/2}$ = 140 Hz, 12H, $-C_6H_3(CF_3)_2$), 4.51 (br s, $\Delta_{1/2}$ = 320 Hz, 36H, $-C(CH_3)_3$), 3.213 (br s, $\Delta_{1/2}$ = 180 Hz, 12H, $-C_6H_2(CH_3)_3$), 0.08 (br s, $\Delta_{1/2}$ = 130 Hz, 4H, $-C_2H_4-$). Magnetic moment (Evans, CD_2Cl_2, 20 °C): μ_{eff} = 2.2 μ_B. Anal. (%) for $C_{74}H_{77}BF_{24}NNiP_2$: calcd. C, 56.69, H, 4.95, N, 0.89; found C, 56.40, H, 5.03, N, 0.82.

Synthesis of [(dtbpe)Ni-NH(dmp)$^+$][B(Ar^F)$_4^-$] (9)

Method A (from [(dtbpe)Ni=N(dmp)$^+$][$B(Ar^F)^-_4$] (**8**) by hydrogen atom addition). To a stirring solution of **8** (80 mg, 0.05 mmol in 5 mL of diethyl ether at room temperature), was added at once a solution of $HSnBu_3$ (15 mg, 0.05 mmol in 1 mL of Et_2O). The mixture turned from dark green to purple. After stirring for 30 min at room temperature, the volatiles were removed under reduced pressure and the residue was triturated three times with 5 mL of *n*-pentane. Pure, crystalline **9** was isolated by cooling a concentrated diethyl ether solution layered with an equal volume of *n*-pentane to −35 °C. Yield: 75 mg, 95%. **Method B** (from (dtbpe)Ni=N(dmp) (**7**) by protonation). A 20-mL scintillation vial was charged with 70.5 mg (0.1 mmol) of (dtbpe)Ni=N(dmp) (**7**) and 5 mL of Et_2O and the solution cooled to −35 °C. A cold solution of [$H(OEt_2)_2^+$][$B(Ar^F)_4^-$] (101 mg, 0.1 mmol in 3 mL of Et_2O at −35 °C) was added with constant stirring and the mixture was allowed to warm up to room temperature. The volatiles were removed under reduced pressure and the dark-purple residue was triturated 3 times with *n*-pentane. Pure, crystalline **9** was isolated by cooling a concentrated diethyl ether solution layered with an equal volume of *n*-pentane to −35 °C. Yield: 140 mg, 90%. The purity of the product was verified by NMR spectroscopy and the data compared to previously reported data.[16]

X-ray Crystal Structure of 2

X-ray quality crystals were obtained by slow crystallization at −35 °C from a concentrated Et_2O solution layered with pentanes. A 0.05 × 0.03 × 0.02 mm^3, purple block was chosen and mounted on the diffractometer. Two independent molecules are present in the unit cell and some of the CF_3 groups present some degree of thermal disorder. This disorder was not modeled. A total of 40000 reflections (−22 ≤ h ≤ 22, −24 ≤ k ≤ 24, −26 ≤ l ≤ 27) was collected at T = 100(2) K with θ_{max} = 28.27°, of which 28323 were unique (R_{int} = 0.0514). The residual peak and hole-electron density were 2.850 and −1.057 eÅ^{-3}. The least-squares refinement converged normally with residuals of R_1 = 0.0981 ($I > 2\sigma(I)$) and GOF of 1.119. Crystal and refinement data for **2**: $C_{60}H_{68}BF_{24}NiP_2$, space group $P\bar{1}$, a = 16.6160(19) Å, b =

19.441(2) Å, c = 20.680(2) Å, α = 95.168°, β = 100.073(2)°, γ = 103.594(2)°, V = 6332.8(12) Å^3, Z = 4, μ = 0.466 mm^{-1}, F(000) = 2856, R_1 = 0.1379, wR_2 = 0.2238 (based on all data).

X-ray Crystal Structure of 3

X-ray quality crystals were obtained by slow crystallization at −35 °C from a concentrated 1,2-$C_6H_4F_2$ solution layered with pentanes. A 0.3 × 0.5 × 0.6 mm^3, dark-purple block was chosen and mounted on the diffractometer. A total of 32564 reflections (−16 ≤ h ≤ 21, −19 ≤ k ≤ 18, −27 ≤ l ≤ 27) was collected at T = 100(2) K with θ_{max} = 25.00°, of which 11176 were unique (R_{int} = 0.0381). The residual peak and hole-electron density were 0.685 and −0.351 eÅ^{-3}. The least-squares refinement converged normally with residuals of R_1 = 0.0717 ($I > 2\sigma(I)$) and GOF of 1.236. Crystal and refinement data for **3**: $C_{60}H_{67}BF_{24}NiP_2$, space group $P2_1/n$, a = 17.736(5) Å, b = 16.476(4) Å, c = 23.481(6) Å, β = 112.082(4)°, V = 6358.5(3) Å^3, Z = 4, μ = 0.465 mm^{-1}, F(000) = 2852, R_1 = 0.0837, wR_2 = 0.1500 (based on all data).

X-ray Crystal Structure of 8

X-ray quality crystals were obtained by slow crystallization at −35 °C from a concentrated pentanes solution. A 0.06 × 0.05 × 0.05 mm^3, olive-green block was chosen and mounted on the diffractometer. A total of 41170 reflections (−18 ≤ h ≤ 18, −17 ≤ k ≤ 10, −49 ≤ l ≤ 52) was collected at T = 100(2) K with θ_{max} = 28.28°, of which 16471 were unique (R_{int} = 0.0774). The residual peak and hole-electron density were 0.775 and −0.439 eÅ^{-3}. The least-squares refinement converged normally with residuals of R_1 = 0.0714 ($I > 2\sigma(I)$) and GOF of 0.972. Crystal and refinement data for **8**: $C_{74}H_{77}BF_{24}NNiP_2$, space group $P2_1/n$, a = 14.2589(12) Å, b = 13.0889(11) Å, c = 39.706(3) Å, β = 90.907(2)°, V = 7409.5(11) Å^3, Z = 4, μ = 0.408 mm^{-1}, F(000) = 3228, R_1 = 0.0775, wR_2 = 0.1433 (based on all data).

DFT Calculations

Gaussian 03 (revision D.02)[39] was used for all reported calculations. The B3LYP (DFT) method was used to carry out the geometry optimizations on the model compounds specified in text using the LANL2DZ basis set. The validity of the true minima was checked by the absence of negative frequencies in the energy Hessian. Tables with atomic coordinates of the optimized geometries can be found in the supportive information.

Supplementary Material

Refer to Web version on PubMed Central for supplementary material.

Acknowledgments

This work was supported by the National Science Foundation through grants CHE-0615274 and CHE-0957816 (to G.L.H.), a Beckman Scholars Fellowship from the Arnold and Mabel Beckman Foundation (to J.S.A.), and a NIH postdoctoral fellowship GM-072291 (to M.P.M.).

REFERENCES

(1). Mindiola DJ, Hillhouse GL. J. Am. Chem. Soc. 2001; 123:4623–4624. [PubMed: 11457258]

(2). Melenkivitz R, Mindiola DJ, Hillhouse GL. J. Am. Chem. Soc. 2002; 124:3846–3847. [PubMed: 11942818]

(3). Mindiola DJ, Hillhouse GL. J. Am. Chem. Soc. 2002; 124:9976–9977. [PubMed: 12188647]

(4). Waterman R, Hillhouse GL. J. Am. Chem. Soc. 2003; 125:13350–13351. [PubMed: 14583018]

(5). Waterman R, Hillhouse GL. Organometallics. 2003; 22:5182–5184.

(6). Harrold ND, Waterman R, Hillhouse GL, Cundari TR. J. Am. Chem. Soc. 2009; 131:12872–12873. [PubMed: 19737011]

(7). Kitiachvili KD, Mindiola DJ, Hillhouse GL. J. Am. Chem. Soc. 2004; 126:10554–10555. [PubMed: 15327309]

(8). Curley JJ, Kitiachvili KD, Waterman R, Hillhouse GL. Organometallics. 2009; 28:2568–2571.

(9). Kogut E, Wiencko HL, Zhang L, Cordeau DE, Warren TH. J. Am. Chem. Soc. 2005; 127:11248–11249. [PubMed: 16089446]

(10). Waterman R, Hillhouse GL. J. Am. Chem. Soc. 2008; 130:12628–12629. [PubMed: 18729364]

(11). Iluc VM, Miller AJM, Hillhouse GL. Chem. Commun. 2005:5091–5093.

(12). Bart SC, Lobkovsky E, Bill E, Chirik PJ. J. Am. Chem. Soc. 2006; 128:5302–5303. [PubMed: 16620076]

(13). Brown SD, Betley TA, Peters JC. J. Am. Chem. Soc. 2003; 125:322–323. [PubMed: 12517130]

(14). Brown SD, Peters JC. J. Am. Chem. Soc. 2005; 127:1913–1923. [PubMed: 15701026]

(15). Gavenonis J, Tilley TD. J. Am. Chem. Soc. 2002; 124:8536–8537. [PubMed: 12121088]

(16). Iluc VM, Hillhouse GL. J. Am. Chem. Soc. 2010; 132:15148–15150. [PubMed: 20929225]

(17). Proulx G, Bergman RG. J. Am. Chem. Soc. 1995; 117:6382–6383.

(18). Proulx G, Bergman RG. Organometallics. 1996; 15:684–692.

(19). Fickes MG, Davis WM, Cummins CC. J. Am. Chem. Soc. 1995; 117:6384–6385.

(20). Guillemot G, Solari E, Floriani C, Rizzoli C. Organometallics. 2001; 20:607–615.

(21). Hanna TA, Baranger AM, Bergman RG. Angew. Chem. Int. Ed. 1996; 35:653–655.

(22). Barz M, Herdtweck E, Thiel WR. Angew. Chem. Int. Ed. 1998; 37:2262–2265.

(23). Dias HVR, Polach SA, Goh S, Archibong EF, Marynick DS. Inorg. Chem. 2000; 39:3894–3901. [PubMed: 11196786]

(24). Albertin G, Antoniutti S, Baldan D, Castro J, Garcia-Fontan S. Inorg. Chem. 2008; 47:742–748. [PubMed: 18078336]

(25). Munro GAM, Pauson PL. J. Organomet. Chem. 1978; 160:177–181.

(26). Gritsan NP, Platz MS. Chem. Rev. 2006; 106:3844–3896. [PubMed: 16967923]

(27). Sur SK. J. Magn. Reson. 1989; 82:169–173.

(28). Evans DF. J. Chem. Soc. 1959:2003–2005.

(29). Carlin, RL.; van Duyneveldt, A. J. Magnetic Properties of Transition Metal Compounds. Springer; Berlin Heidelberg, New York: 1977.

(30)(a). Carlin, RL. Magneto-chemistry. Springer-Verlag; Berlin Heidelberg New York: 1986. (b) Henry WE. Phys Rev. 1952; 88:559.(c) Casimir, HBG. Magnetism and Very Low Temperatures. Dover Publications; New York: 1961.

(31). Bai G, Stephan DW. Angew. Chem. Int. Ed. 2007; 11:1856–1859.

(32)(a). Buttner T, Geier J, Frison G, Harmer J, Calle C, Schweiger A, Schonberg H, Grützmacher H. Science. 2005; 307:235–238. [PubMed: 15653498] (b) Nieto I, Ding F, Bontchev RP, Wang H, Smith JM. J. Am. Chem. Soc. 2008; 130:2716–2717. [PubMed: 18266366] (c) King ER, Hennessy ET, Betley TA. J. Am. Chem. Soc. 2011; 133:4197–4123.

(33). For $^{n}Bu_3SnH$, the Sn-*H* BDE is ~ 74 kcal/mol.[33a] For $O(CH_2CH_3)_2$, the C-*H* BDE is ~ 93 kcal/mol.[33b] (a)Davies AG. Organotin Chemistry (2nd Ed). 2004Wiley-VCHWeinheim (b) McMillen DF, Golden DM. Ann. Rev. Phys. Chem. 1982; 33:493–532.

(34). Pangborn AB, Giardello MA, Grubbs RH, Rosen RK, Timmers FJ. Organometallics. 1996; 15:1518–1520.

(35). Schwindt MA, Lejon T, Hegedus LS. Organometallics. 1990; 9:2814–2819.

(36). Chavez I, Alvarez-Carena A, Molins E, Roig A, Maniukiewicz W, Arancibia A, Arancibia V, Brand H, Manriquez JM. J. Organomet. Chem. 2000; 601:126–132.

(37). Bach I, Porschke K, Goddard R, Kopiske C, Kruger C, Rufinska A, Seevogel K. Organometallics. 1996; 15:4959–4966.

(38). All software and sources of scattering factors are contained in the SHELXTL (version 5.1) program library (G. Sheldrick, Bruker Analytical X-ray Systems, Madison, WI).

(39). Frisch, MJ., et al. Gaussian, Inc.; Wallingford CT: 2004.

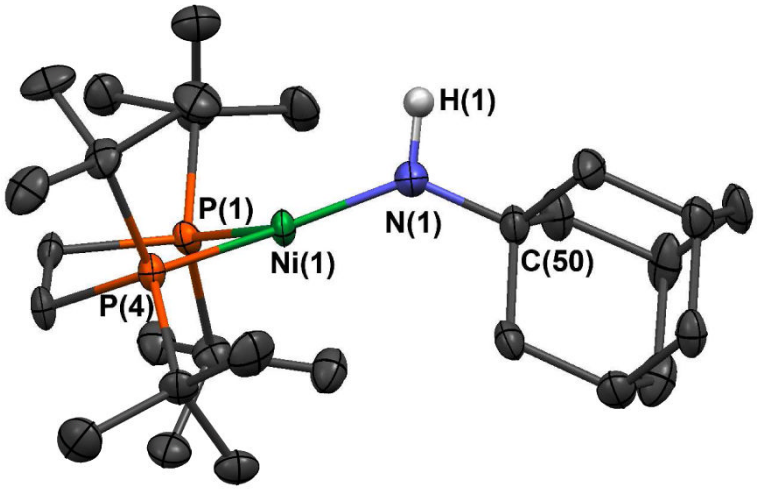

Figure 1.

Thermal-ellipsoid (50% probability) representation of the complex cation of **2** (only one of the two independent molecules from the unit cell is shown; irrelevant H atoms omitted for clarity). Selected metrical parameters: Ni(1)–N(1) = 1.771(4), P(1)–Ni(1) = 2.1609(14), P(4)–Ni(1) = 2.1726(14), N(1)–C(50) = 1.459(7), N(1)–H(1) = 0.98(4) Å; P(1)–Ni(1)–P(4) = 90.04(5), P(1)–Ni(1)–N(1) = 127.56(16), P(4)–Ni(1)–N(1) = 141.57(16), Ni(1)–N(1)–C(50) = 134.6(4), Ni(1)–N(1)–H(1) = 115(2), C(50)–H(1)–N(1) = 107(2)°.

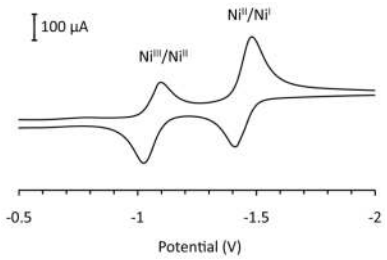

Figure 2.
Cyclic voltammogram of (dtbpe)Ni=NAd (**1**), 10 mM in 0.3 M [$^{n}Bu_4N$][PF_6] in DFB, Cp_2Fe/Cp_2Fe^+ corrected.

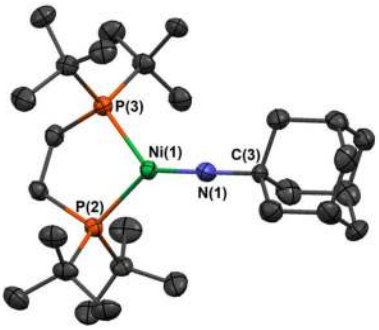

Figure 3.

Thermal-ellipsoid (50% probability) representation of the complex cation of **3**(irrelevant H atoms omitted for clarity). Selected metrical parameters: Ni–N = 1.657(5), P(2)–Ni = 2.1992(12), P(1)–Ni = 2.2041(12), N–C(3) = 1.424(7) Å; P(2)–Ni–P(1) = 91.17(5), P(2)–Ni–N = 132.28(13), P(1)–Ni–N = 135.94(13), Ni–N–C(3) = 165.2(4)°.

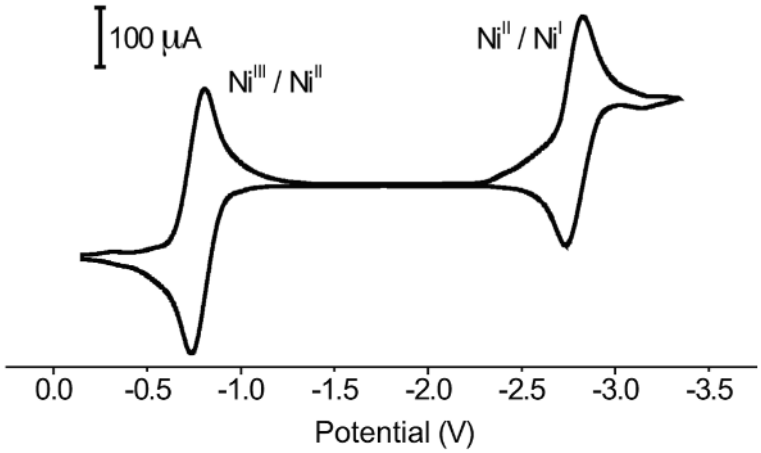

Figure 4.
Cyclic voltammogram of (dtbpe)Ni=N(dmp) (**7**) at 150 mV/s, 10 mM in 0.3 M [$^{n}Bu_4N$][$PF_6$6] in THF, Cp_2Fe/Cp_2Fe^+ corrected.

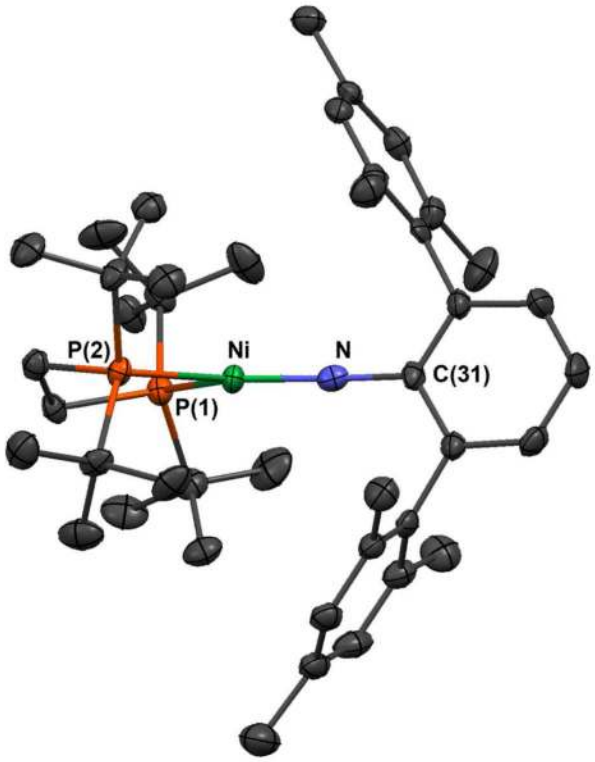

Figure 5.

Thermal-ellipsoid (50% probability) representation of the complex cation of **8** (irrelevant H atoms omitted for clarity). Selected metrical parameters: Ni–N = 1.674(3), Ni–P(1) = 2.2314(11), Ni–P(2) = 2.2318(11), N–C(31) = 1.359(5) Å; Ni–N–C(31) = 178.4(3), P(1)–Ni–P(2) = 90.37(2), P(1)–Ni–N = 133.81(10), P(2)–Ni–N = 135.82(10)°.

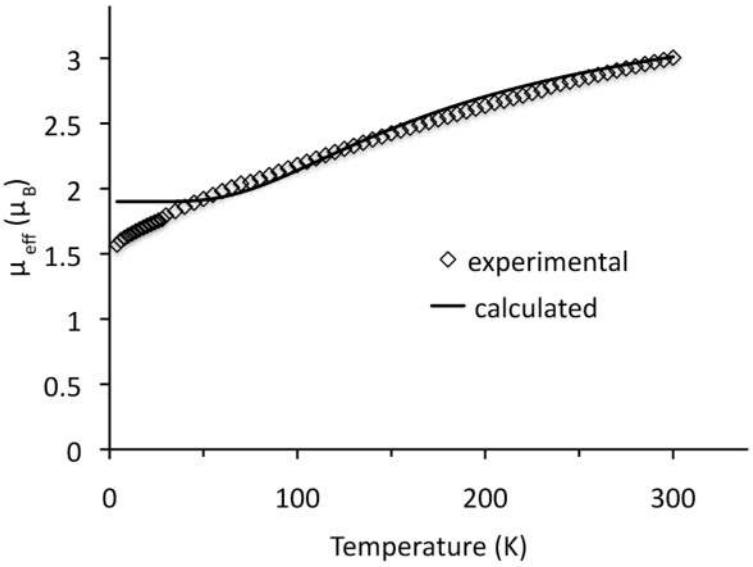

Figure 6.
Plot of magnetic moment versus temperature for solid [(dtbpe)NiNAd^{+}][B(Ar^{F})$_4^{-}$] (**3**). The solid line represents the fitted data for the two spin states equilibrium mixture.

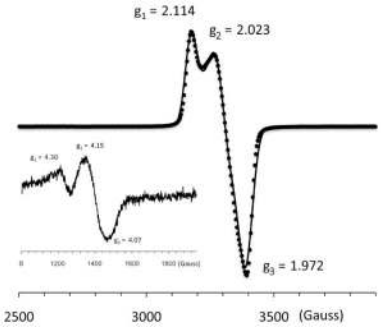

Figure 7.
EPR spectrum of **3** (3.5 mM frozen glass in CH_2Cl_2, 3.7 K); the solid line represents the simulated spectrum.

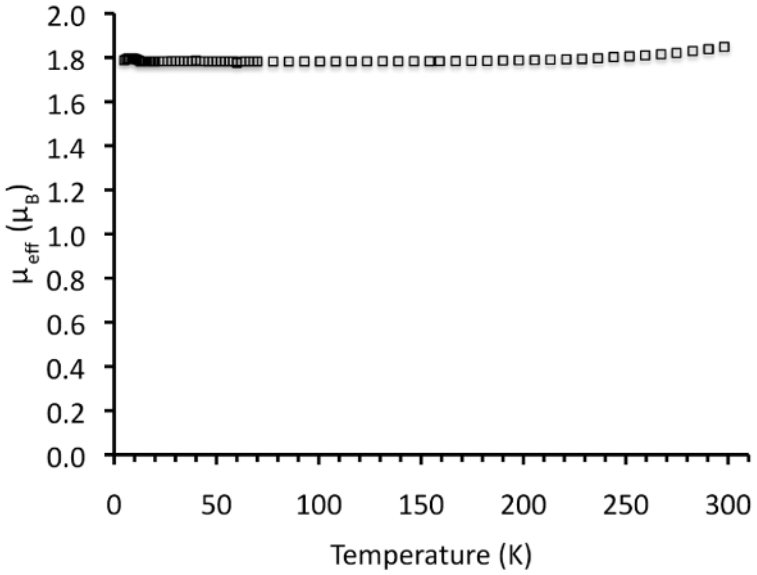

Figure 8.
Plot of magnetic moment versus temperature for solid [(dtbpe)Ni=N(dmp)$^{+}$][B(Ar^{F})$_4^{-}$] (**8**).

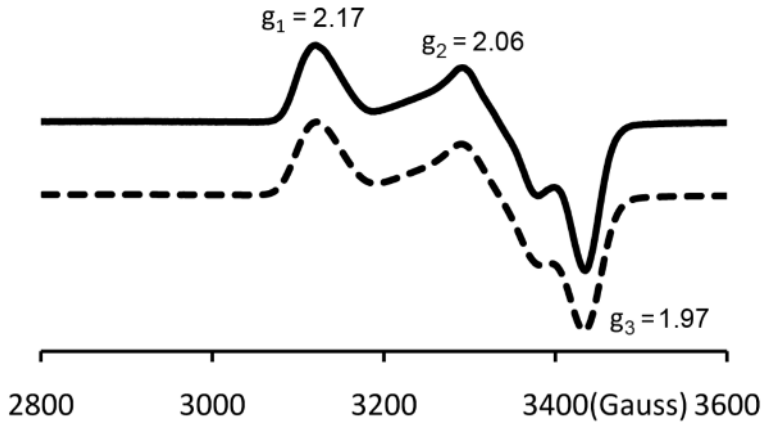

Figure 9.
EPR spectrum (frozen glass 1.0 mM in toluene) for **8**: experimental, 4 K (solid line) and simulated (dashed line).

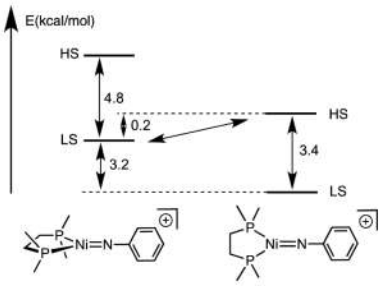

Figure 10.
Diagram with free-energy differences (kcal/mol) between the low- and high-spin states for [(dmpe)Ni=NPh^{+}]; left: the rotamer with the imide phenyl ring perpendicular to the PNiP plane; right: the rotamer with the imide phenyl ring coplanar to the PNiP plane.

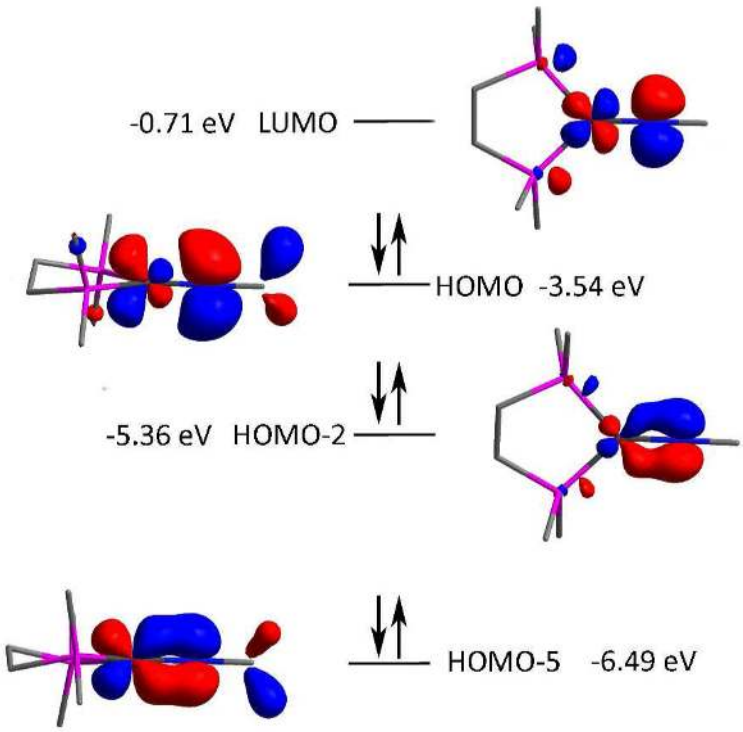

Figure 11.
Frontier molecular orbitals for a (dmpe)Ni=N^{t}Bu model showing the orbital interactions between nickel and the nitrogen imide.

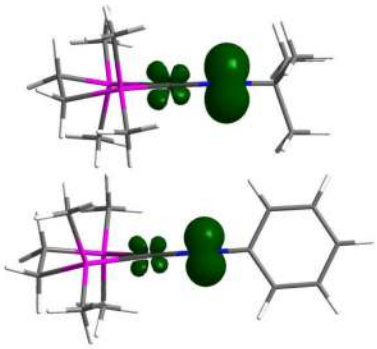

Figure 12.
Spin-density plot for [(dmpe)Ni=NC(CH_3)$_3^+$] (top) and [(dmpe)Ni=NPh$^+$] models (bottom).

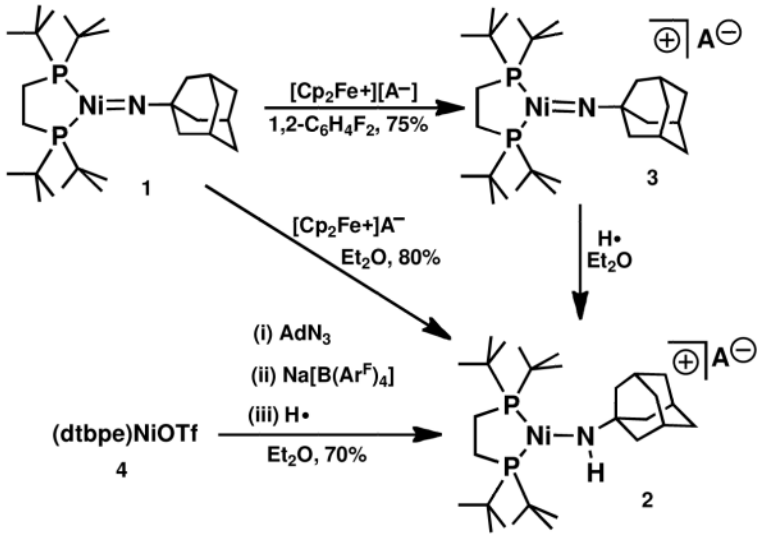

Scheme 1.
Synthesis of the adamantyl-substituted Ni(III) imide (**3**) $[A^-] = [B(Ar^F)_4^-]$.

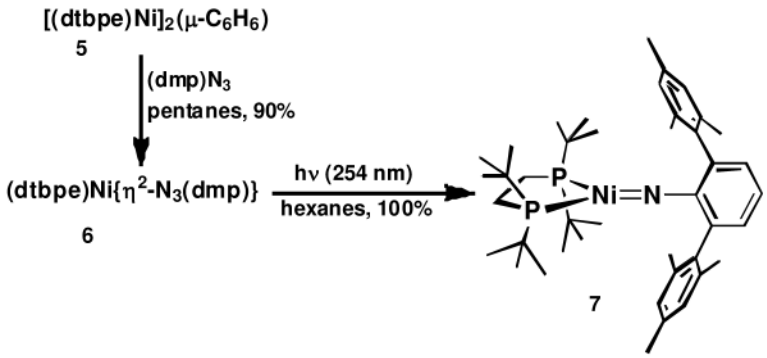

Scheme 2.
Organoazide Route for the Synthesis of (dtbpe)Ni=N(dmp) (**7**).

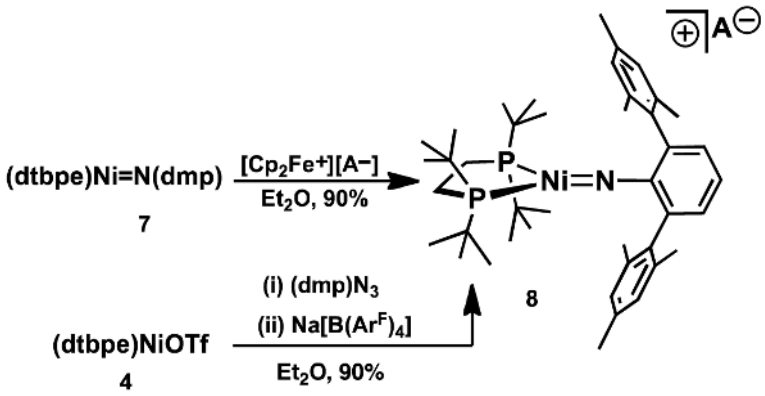

Scheme 3.
Synthesis of [(dtbpe)Ni=N(dmp)$^{+}$][B(Ar^{F})$_4$$^{-}$] (**8**); [A^{-}] = [B(Ar^{F})$_4$$^{-}$].

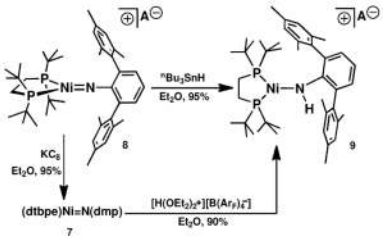

Scheme 4.
Reactivity of **8**; $[A^-] = [B(Ar^F)_4^-]$.